

Constraining flavour-universal nonstandard interactions and superweak extension of the standard model

Timo J. Kärkkäinen*

*Laboratory of High Energy and Computational Physics,
National Institute of Chemical Physics and Biophysics,
Rävala pst. 10, 10143 Tallinn, Estonia*

Zoltán Trócsányi†

*Institute for Theoretical Physics, ELTE Eötvös Loránd University,
Pázmány Péter sétány 1/A, 1117 Budapest, Hungary
ELKH-DE Particle Physics Research Group,
4010 Debrecen, PO Box 105, Hungary*

Abstract

Nonstandard neutrino interactions (NSI) arising from light and heavy mediators probe different sectors of the parameter space of models focusing on phenomena that require the extension of the standard model. High-energy scattering experiments are not relevant on constraining the NSI hiding a light mediator at the fundamental level, while flavour-universal NSI cannot be probed with neutrino oscillation experiments. Currently the only way to measure flavour-universal NSI with a light mediator is to rely on coherent elastic neutrino-nucleon scattering experiments, which we use to derive bounds for light mediator flavour-universal NSI. For light NSI, we obtain $\varepsilon^u \in [-14.85, 14.79]$ and $\varepsilon^d = [-13.19, 13.84]$ (90 % CL.). We also derive constraints on flavour-universal heavy NSI and find a 2σ tension. Finally, we discuss the implications of the experiments on the allowed parameter space of a specific example model, called superweak extension of the standard model.

I. INTRODUCTION

The discovery of neutrino oscillations [1, 2] kickstarted a plethora of research efforts in neutrino physics. As the standard model (SM) is devoid of neutrino masses, neutrinos are an exciting option as a portal to new physics, which must contain a mechanism to generate neutrino masses, and therefore neutrino oscillations. One of the most popular models of mass generation is the seesaw mechanism [3–14]. The type I mechanism introduces heavy right-handed neutrinos that are sterile under the SM. As at least two of the three active neutrinos are massive, the minimum extension includes two sterile neutrinos. In this paper we focus on the type I mechanism; see Refs. [15–17] for reviews on other types of neutrino mass generation mechanisms.

New physics effects are manifested at low energy scales via effective operators, which are generated by integrating out the heavy degrees of freedom from the high-energy

* karkkainen@kbfj.ee

† zoltan.trocsanyi@cern.ch

theory. In the context of neutrino physics, there are three important operators:

$$\mathcal{O}_5 = \frac{C_5}{\Lambda} (\bar{L}^c \cdot H)(H \cdot L), \quad (1)$$

$$\mathcal{O}_{6a} = \frac{C_{6a}}{\Lambda^2} (\bar{L} \gamma^\mu P_L L)(\bar{f} \gamma_\mu P_X f), \quad (2)$$

$$\mathcal{O}_{6b} = \frac{C_{6b}}{\Lambda^2} (\bar{L} \cdot H) i \not{\partial} (H^\dagger \cdot L) \quad (3)$$

where the dot represents the $SU(2)_L$ invariant product of doublets and Λ is the scale of new physics. The first operator is the Weinberg operator [18], which is the only possible gauge invariant dimension-5 operator that can be constructed from the SM fields. After spontaneous symmetry breaking this gives a Majorana neutrino mass term. The second operator corresponds to *nonstandard interactions* (NSIs) [19] of four charged leptons or charged lepton – quark NSI that in general break flavour. The third operator arises from active-sterile neutrino mixing. The latter two operators are of dimension six.

The scale Λ is interpreted as the energy scale of new physics, typically considered much higher than the electroweak scale, corresponding to a *heavy NSI mediator* at the fundamental level. This expectation is based on the assumption that the couplings C_i are $\mathcal{O}(1)$ coefficients. However, quantum field theory does not *a priori* force the couplings to be so large. In the SM, a prime example of small couplings is the Yukawa coupling of the electron, $y_e \simeq 3 \cdot 10^{-6} \ll 1$. In the case when the couplings $C_i \ll 1$, the scale Λ can be as low as GeV or even MeV, and the mass of the corresponding NSI mediator may be light or similar when compared to the momentum transfer in the experiment. While such scenarios do not support models built on naturalness arguments, they are certainly not ruled out, and also predictive. Such new physics interactions can be probed at high-intensity, low-energy experiments that are planned for the next decades, at the European Spallation Source [20] (ESS) for example. The ESS promises an order of magnitude increase in neutrino flux as compared to that of the Spallation Neutron Source where the first successful detection of coherent elastic neutrino-nucleon scattering (CE ν NS) [21] was carried out by the COHERENT experiment [22, 23]. The increase in statistics is the key to improve the bounds on the NSI parameters.

Neutrino interactions have very low cross sections. Nonetheless neutrino-electron and neutrino-nucleon cross sections have been measured at scattering experiments where the averaged momentum transfer squared is large, $\langle q^2 \rangle = 20 \text{ GeV}^2$ [24–26]. These measurements give stringent bounds to new physics effects originating from the effective

operators, namely the NSI with new physics scale $\Lambda > \Lambda_{\text{EW}}$. The observation of $\text{CE}\nu\text{NS}$ by COHERENT allows us to test whether or not NSI effects exist with scale Λ significantly below the electroweak scale.

Different extensions of the SM produce different NSI textures. A subclass of these extensions is flavour conserving. Consequently, the NSI matrix is diagonal and real, containing only three elements, which have contributions from up-type quarks, down-type quarks and charged leptons. If in addition the extension is flavour universal, then the NSI matrix is isotropic (proportional to the unit matrix). In the bottom-to-top approach, current experimental bounds can be used to constrain the high-energy theory parameters. In contrast, the top-to-bottom approach can be used to predict the texture and region NSI available for a particular UV complete model.

In this paper, we discuss the NSI formalism and both approaches by considering the constraints with light and heavy NSI mediators. We derive bounds for flavour-universally coupled NSI mediator in *both the light and the heavy case*. We consider a specific example, the super-weak extension of the standard model (SWSM) [27] which exhibits tiny flavour-universal couplings to fermions. A similar study but in the context of different models has been recently carried out [28]. The SWSM contains an NSI mediator that is light in scattering experiments and therefore it evades detection, but not so in $\text{CE}\nu\text{NS}$, which is sensitive for NSI originating from SWSM. We derive bounds on the new gauge coupling and ratio of the vacuum expectation values in the SWSM based on the results of COHERENT [22, 23, 29] and our previous analyses on dark matter [30] in the SWSM.

Our paper is organized as follows. We introduce the NSI formalism in Section II and present the bounds for flavour-universal NSI parameters in the case of light and heavy mediator. We then discuss in Section III a particular example of a model which exhibits flavour-universal NSI — the superweak extension of the standard model. In Section IV we present our results: on one hand, the bounds from COHERENT constrain the gauge parameters of the superweak extension, while on the other the properties of the model predict texture and correlations for the NSI parameters. We present our conclusions in Section V.

II. EXPERIMENTAL CONSTRAINTS ON THE NSI PARAMETERS

A. NSI formalism

In our study we focus on the \mathcal{O}_{6a} operator of Eqn. (2) that is relevant to neutrino-matter interactions. In the usual parametrization of the NSI Lagrangian the interaction strength is set by the Fermi coupling G_F ,

$$\mathcal{L}_{\text{NSI}} = -2\sqrt{2}G_F \sum_{f,X=\pm,\ell,\ell'} \varepsilon_{\ell,\ell'}^{f,X} (\bar{\nu}_\ell \gamma^\mu P_L \nu_{\ell'}) (\bar{f} \gamma_\mu P_X f) \quad (4)$$

where $\varepsilon_{\ell,\ell'}^{f,X}$ parametrizes the strength of the new interaction with respect to G_F , with ℓ, ℓ' denoting charged lepton flavours and f being a charged fermion in the standard model.

When one matches the NSI Lagrangian (4) with the effective Lagrangian obtained from a high-energy theory, the NSI parameters are proportional to the propagator of the mediator, i.e. to $\varepsilon_{\ell,\ell'}^{f,X} \propto (q^2 - M^2)^{-1}$, where q^μ is the four-momentum ($q^2 = q_\mu q^\mu$) carried by the mediator and M is its mass. In a neutrino scattering experiment, we may approximate the propagator either as

$$\varepsilon_{\ell,\ell'}^{f,X} \propto +\frac{1}{q^2} \text{ if } q^2 \gg M^2, \quad (5)$$

or

$$\varepsilon_{\ell,\ell'}^{f,X} \propto -\frac{1}{M^2} \text{ if } q^2 \ll M^2. \quad (6)$$

The first case in Eq. (5) corresponds to “light NSI mediator”, while the second one to “heavy NSI mediator”. For concreteness, let us consider $M = 50$ MeV. Then the mediator is considered *heavy* from the *viewpoint of neutrino oscillation experiments*, but *light for high-energy neutrino scattering experiments*, such as CHARM [24] and NuTeV [25]. However, if q^2 is similar in size to M^2 , as in the case of CE ν NS in our example, we cannot take any of these limits. Nevertheless, we can still apply the NSI formalism using the full propagator with q^2 being the characteristic momentum transfer squared in the scattering experiment. The resulting NSI couplings interpolate smoothly between the light and heavy limits. We present an example in Sect. IV B.

B. Global fit of the heavy NSI parameters

Most studies reporting the bounds on NSI parameters simplify the fitting procedure to contain only one nonvanishing NSI parameter. For flavour-universal models these bounds can not be considered, and a global fit instead is required. This has been performed in Refs. [29, 31] for example.

The χ^2 -fitting in [29] follows the standard procedure, where the function

$$\chi^2 = \sum_i \left(\frac{N_i^{\text{exp}} - (1 + \alpha_c)N_i^{\text{theor}} + (1 + \beta_c)B_i}{\sigma_i} \right)^2 + \left(\frac{\alpha_c}{\sigma_{\alpha_c}} \right)^2 + \left(\frac{\beta_c}{\sigma_{\beta_c}} \right)^2 + \left(\frac{\eta_c - 1}{\sigma_{\eta_c}} \right)^2 \quad (7)$$

is minimized with respect to the nuisance parameters α_c , β_c and η_c , corresponding to the systematic uncertainties due to the signal rate, the background rate and a quenching factor. The factors σ_{α_c} , σ_{β_c} , σ_{η_c} are the corresponding standard deviations, and the σ_i are the uncertainties of the number of events in an energy bin N_i^{exp} from Ref. [22], and N_i^{theor} is the theory estimate in the same bin.

In Ref. [31] the authors perform a global fit to current experiments for the NSI couplings with heavy mediators and in the absence of CP violation, that is, the NSI parameters are assumed to be real. The authors performed a χ^2 -test (their procedure for COHERENT assumes only one nuisance factor, and the analysis predates the start of COHERENT experiment), minimizing the χ^2 -function, and presented the dependence of the $\Delta\chi^2$ -distributions (the difference of a χ^2 -test value to χ^2 best-fit value), that is, the statistical significance of the NSI parameters. We reproduced those plots here in Fig. 1, with 2σ and 90% confidence intervals exhibited. We read off the best-fit points directly from these graphs, and presented those together with the confidence intervals in Table I.

We then combined the individual $\Delta\chi^2$ -distributions to test flavour-universal couplings by summing the three $\Delta\chi^2$ -distributions [32]:

$$\Delta\chi_{\text{isotropic}}^2 = \Delta\chi_{ee}^2 + \Delta\chi_{\mu\mu}^2 + \Delta\chi_{\tau\tau}^2. \quad (8)$$

We present the combined up- and down-type isotropic heavy NSI coupling $\Delta\chi^2$ -distributions in Fig. 2, with the individual original distributions overlaid. The relative incompatibility of different flavour distributions results in tension with experimental data indicating that both the up- and down-type quark isotropic NSI scenario are excluded at 2σ . We compare the individual and combined bounds in Fig. 3. For isotropic

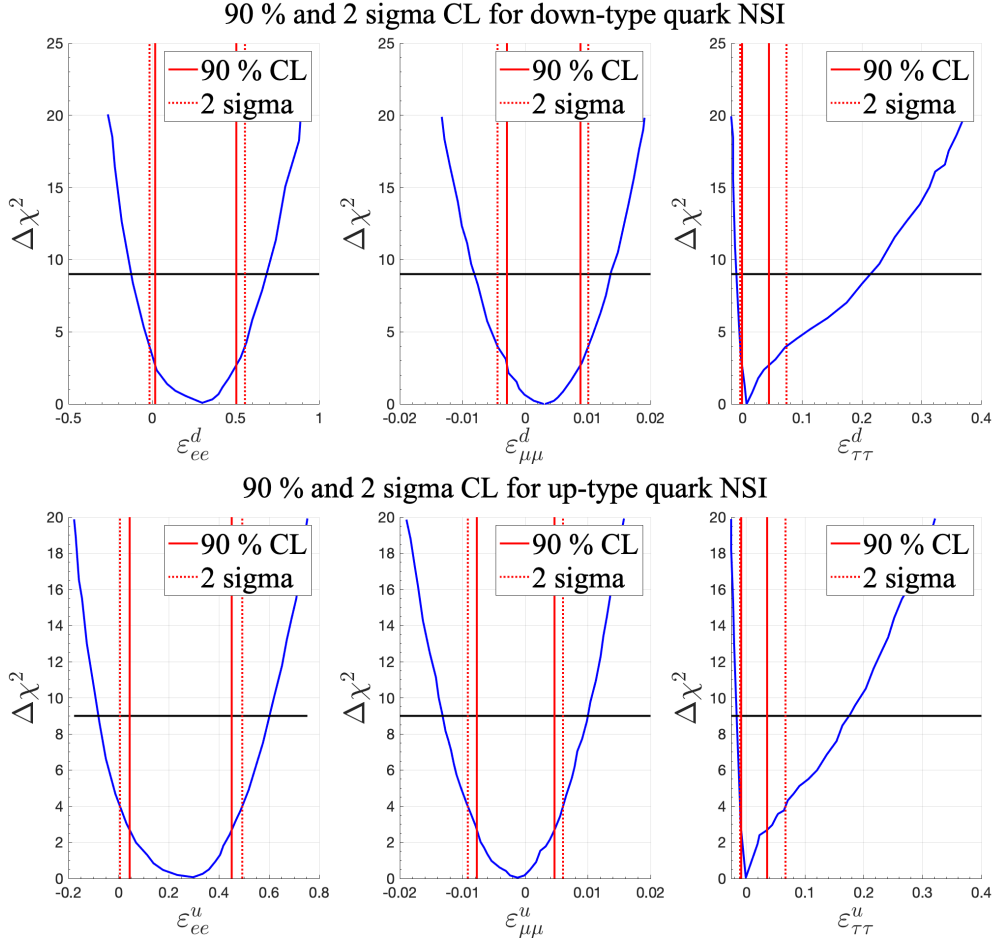


Figure 1. Determinations of 2σ and 90 % confidence intervals from minimized $\Delta\chi^2$ -distributions given in [31]. Down-type quark NSI above and up-type quark NSI below. The vertical black line ($\Delta\chi^2 = 9$) corresponds to the 3σ bound, used to find the values in Table II.

NSI we have summarized our results in Table II. These bounds are relevant for theories which are accessible via high-energy experiments, where the mediator has at least a mass of $\mathcal{O}(10)$ GeV and couples to quark flavours universally.

For leptonic NSI, one can use the constraints given in Fig. 2 of Ref. [33], where the authors performed both one-parameter- and flavour-conserving fits. Their χ^2 -analysis takes into account the data from LEP experiments (ALEPH, DELPHI, L3 and OPAL), LSND experiment, reactor experiments (MUNU and Rovno) and CHARM II experiment. The Borexino experiment has performed one-parameter fits [34] leading to the loosest bound.

Parameter	Best-fit point μ_i	2σ CI $\sigma_{2,i}$	90 % CI $\sigma_{90,i}$
ε_{ee}^d	0.301	[-0.015, 0.556]	[0.019, 0.504]
$\varepsilon_{\mu\mu}^d$	0.003	[-0.004, 0.010]	[-0.003, 0.009]
$\varepsilon_{\tau\tau}^d$	0.006	[-0.004, 0.073]	[-0.001, 0.044]
ε_{ee}^u	0.297	[0.006, 0.493]	[0.044, 0.451]
$\varepsilon_{\mu\mu}^u$	-0.001	[-0.009, 0.006]	[-0.008, 0.005]
$\varepsilon_{\tau\tau}^u$	-0.001	[-0.011, 0.067]	[-0.009, 0.035]

Table I. Best-fit points for diagonal quark NSI parameters, and also 90 % and 2σ confidence intervals (CI) derived from using Fig. 4 of [31]. The bounds apply only for heavy mediator NSI ($M^2 \gg 20 \text{ GeV}^2$).

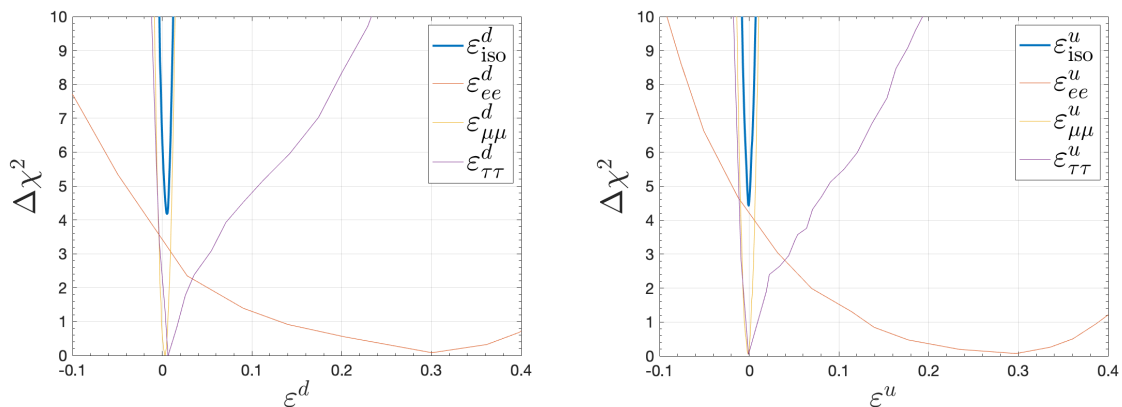


Figure 2. Combined χ^2 -distributions and the individual components overlaid.

C. Flavour universal NSI from the COHERENT experiment

For obtaining constraint on light NSI parameters oscillation experiments can be utilized. However, those cannot observe the diagonal elements of the NSI matrix themselves. Instead, they measure off-diagonal couplings and differences of the diagonal couplings. In Ref. [35] the authors have chosen the convention that $\varepsilon_{\mu\mu}$ is subtracted from the effective Mikheyev-Smirnov-Wolfenstein neutrino oscillation Hamiltonian as a phase rotation, so the observable parameters are $\varepsilon_{ee}^f - \varepsilon_{\mu\mu}^f$ and $\varepsilon_{ee}^f - \varepsilon_{\tau\tau}^f$. Consequently, flavour-conserving NSI (that is, diagonal NSI matrix) can be detected in neutrino oscillations only if it is not flavour- universal. In flavour-universal case the NSI matrix

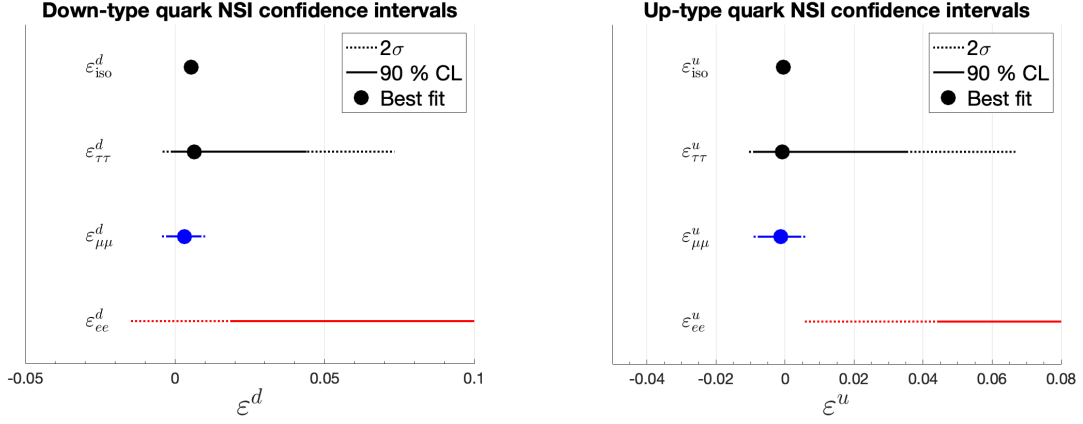


Figure 3. Comparisons of 2σ and 90 % confidence intervals for the diagonal elements, including best-fit value. Left: down-type quark NSI, right: up-type quark NSI. Isotropic NSI included. The best-fit of ε_{ee} is not visible at this range.

Parameter	Best fit	3σ CI
ε^u	-5.5×10^{-4}	$[-0.0073, 0.0063]$
ε^d	5.3×10^{-3}	$[-0.0026, 0.0114]$

Table II. Best-fit points and 3σ confidence intervals for isotropic NSI. The constraints from high-energy experiments have been taken into account, hence the bounds apply only for heavy mediator NSI ($M^2 \gg 20 \text{ GeV}^2$).

is isotropic and manifests itself as an unphysical phase rotation, undetectable in such experiments.

Another resource to test the light NSI couplings is coherent elastic neutrino-nucleon scattering ($\text{CE}\nu\text{NS}$). In this experiment the differential cross section in the recoil energy T ($T \lesssim 10 \text{ keV}$) of the nucleus in this process is given by

$$\frac{d\sigma}{dT} = \frac{G_F^2 M}{\pi} \left(1 - \frac{|\mathbf{q}|^2}{4E_\nu^2}\right) Q_W^2 \quad (9)$$

where M is the mass of the nucleus and $|\mathbf{q}|^2 = 2MT$ is the momentum transfer squared. E_ν is the energy of the neutrino, while Q_W denotes the weak charge for a nucleus of Z protons and N neutrons, which in the standard model reads as

$$Q_W^{\text{SM}} = g_V^n N F_n(\mathbf{q}) + g_V^p Z F_p(\mathbf{q}), \quad g_V^n = -\frac{1}{2}, \quad g_V^p = \frac{1}{2} - 2 \sin^2 \theta_W. \quad (10)$$

The functions F_n and F_p are nuclear form factors for the neutron and the proton

distribution in the nucleus, parameterized using Helm's parameterization in Ref. [29]:

$$F_x(|\mathbf{q}|) = \frac{3j_1(|\mathbf{q}|R_{x,0})}{|\mathbf{q}|R_{x,0}} e^{-|\mathbf{q}|^2 s^2/2}, \quad R_{x,0}^2 = 5s^2 - \frac{5}{3}R_x^2, \quad x = n \text{ or } p. \quad (11)$$

In this formula $R_{x,0}$ is obtained using the surface thickness $s = 0.9$ fm and the the root mean square radii of the proton and neutron distributions inside the nucleus. For instance, $R_p(^{133}\text{Cs}) = 4.804$ fm and $R_n(^{133}\text{Cs}) = 5.01$ for Cesium and $R_p(^{127}\text{I}) = 4.749$ fm and $R_n(^{127}\text{Cs}) = 4.94$ for Iodine used in the experiments. The function $j_1(x) = \frac{\sin x}{x^2} - \frac{\cos x}{x}$ is the spherical Bessel function of the first kind, order 1.

CE ν NS was predicted by Freedman in 1974 [21], and finally observed for the first time in COHERENT experiment in 2017 [22]. The first run used Cesium-133 and Iodine-127 nuclei in 2017 and the second run liquid Argon- 40 in 2020[23].

The generalization of the weak charge in Eq. (10) to the case of generic NSI is

$$\begin{aligned} Q_{W,e}^2 = & (g_V^p + 2\varepsilon_{ee}^u + \varepsilon_{ee}^d)ZF_p(|\mathbf{q}|) + (g_V^n + \varepsilon_{ee}^u + 2\varepsilon_{ee}^d)NF_n(|\mathbf{q}|))^2 \\ & + |(2\varepsilon_{e\mu}^u + \varepsilon_{e\mu}^d)ZF_p(|\mathbf{q}|) + (\varepsilon_{e\mu}^u + 2\varepsilon_{e\mu}^d)NF_n(|\mathbf{q}|)|^2 \\ & + |(2\varepsilon_{e\tau}^u + \varepsilon_{e\tau}^d)ZF_p(|\mathbf{q}|) + (\varepsilon_{e\tau}^u + 2\varepsilon_{e\tau}^d)NF_n(|\mathbf{q}|)|^2 \end{aligned} \quad (12)$$

where $\varepsilon_{\ell\ell'}^f = \varepsilon_{\ell\ell'}^{f,+} + \varepsilon_{\ell\ell'}^{f,-}$.

We remark that the leading order contribution to the flavour- breaking NSI parameters $\varepsilon_{\ell\ell'}^f$ ($\ell \neq \ell'$) is proportional to the second order of those parameters, while the flavour-conserving parameters contribute at both first and second order (linear and square terms). If both flavour- conserving and flavour-breaking NSI parameters have approximately the same magnitude and are significantly less than one, then we may neglect the second order terms. Then, the flavour-conserving NSI parameters dominate the distortion to the weak charge Q_W^2 :

$$\begin{aligned} Q_{W,e}^2 = & Q_{W,e}^{\text{SM}} \\ & + 2(g_V^n)^2 (\varepsilon_{ee}^u + 2\varepsilon_{ee}^d) N^2 F_n^2 + 6g_V^n g_V^p (\varepsilon_{ee}^u + \varepsilon_{ee}^d) N Z F_n F_p + 2(g_V^p)^2 (2\varepsilon_{ee}^u + \varepsilon_{ee}^d) Z^2 F_p^2. \end{aligned} \quad (13)$$

Presently large values (larger than one) for the light NSI parameters are still allowed experimentally for both flavour- conserving and flavour-breaking case [29]. In such a case, one should use the complete formula for the weak charge as given in Eq. (12).

We may utilize the COHERENT limit given by [29] to constrain ε_{ee}^q . Analogously, the same argument can be used to demonstrate the dominance of the $\mu\mu$ elements on $Q_{W,\mu}^2$.

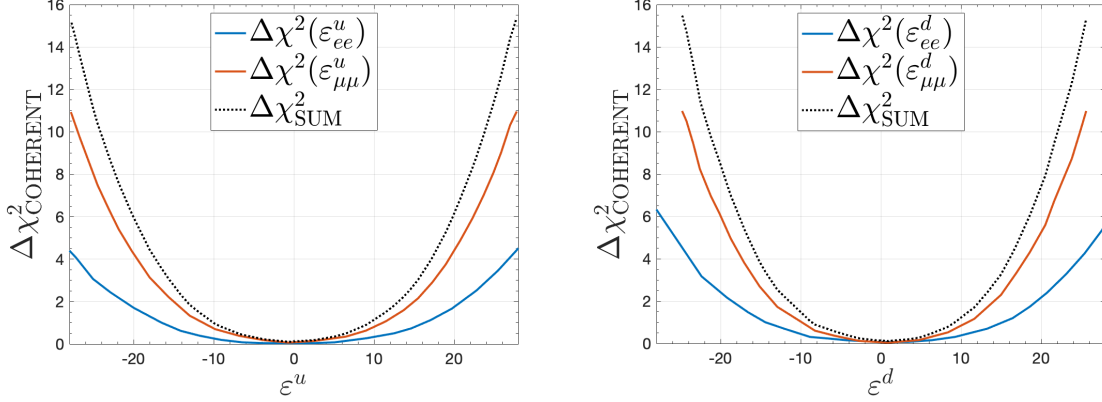


Figure 4. Combined $\Delta\chi^2$ -distributions and the individual components overlaid. Only COHERENT data is taken into account.

We performed the combination of $\Delta\chi^2$ -distributions also for COHERENT experiment, which is sensitive to $\varepsilon_{ee}^q, \varepsilon_{e\mu}^q$ and $\varepsilon_{\mu\mu}^q$ but not to $\varepsilon_{\tau\tau}^q$, where $q = u, d$. In isotropic NSI models $\varepsilon_{ee}^q = \varepsilon_{\mu\mu}^q$. We assume the COHERENT measurements of these two couplings to be independent and sum the $\Delta\chi^2$ -distributions related to these parameters, following the instruction of Ref. [32]. We then derive the COHERENT bounds for isotropic NSI parameters. We reproduce the individual $\Delta\chi^2$ -distributions taken from Ref. [29], and show them together with the combination in Fig. 4. The corresponding confidence intervals are given in Table III.

Parameter	2σ CI	90 % CI	1σ CI
ε^u	[-17.25, 17.16]	[-14.85, 14.79]	[-10.01, 9.42]
ε^d	[-15.31, 16.05]	[-13.19, 13.84]	[-8.61, 9.23]

Table III. Confidence intervals for isotropic NSI couplings based on the COHERENT constraints.

A somewhat similar analysis in Ref. [36] has provided bounds for both diagonal and non-diagonal NSI couplings for up- and down-type quarks. It has been completed with the assumption that NSI coupling is the same for both oscillation and CE ν NS experiments. This is true if the momentum transfer $q^2 \ll M^2$, where M is the NSI mediator mass (heavy NSI mediator). However, in the case of light NSI this condition does not hold. Our analysis is performed in the region where the NSI coupling is

Field	Q_L	u_R	d_R	L_L	ℓ_R	N_R
$U(1)_z$ charge	$\frac{1}{6}$	$\frac{7}{6}$	$-\frac{5}{6}$	$-\frac{1}{2}$	$-\frac{3}{2}$	$\frac{1}{2}$

Table IV. Charges of the extra $U(1)$ symmetry of the fermions in SWSM.

$g^2/(q^2 - M^2)$, in contrast to oscillations, where the coupling is g^2/q^2 .

III. NSI COUPLINGS DERIVED IN THE SWSM

In this section we provide an example of a model that naturally yields an isotropic NSI matrix, namely, the super-weak extension of the standard model [27]. We recall the details of the SWSM only to the extent needed to derive the NSI couplings. For more details on the model, we call attention to Refs. [30, 37–39] where various phenomenological aspects were studied.

A. Super-weak extension of the standard model

The SWSM is based on the $SU(3)_c \otimes SU(2)_L \otimes U(1)_Y \otimes U(1)_z$ gauge group. The $U(1)$ gauge couplings are denoted by g_y and g_z . The anomaly-free $U(1)_z$ charges for the fermions are presented in Table IV. The $SU(2)_L \otimes U(1)_Y$ symmetry is broken by the vacuum expectation value v of the usual Brout-Englert-Higgs field, while the $U(1)_z$ symmetry is spontaneously broken by the vacuum expectation value w of a complex scalar singlet (under transformations of the SM), making the corresponding neutral gauge bosons Z and Z' massive. These bosons mix weakly with mixing angle θ_Z .

The covariant derivative related to the Abelian sector of the model is

$$D_\mu \supset D_\mu^{U(1)} = \partial_\mu - i(y, z) \begin{pmatrix} g_y & -\eta g_z \\ 0 & g_z \end{pmatrix} R_\epsilon \begin{pmatrix} B_\mu \\ B'_\mu \end{pmatrix} \quad (14)$$

where R_ϵ is an unphysical rotation matrix (whose rotation angle can be absorbed in θ_Z), y and z are the $U(1)$ charges, and the parameter η is a convenient way to parametrize the kinetic mixing between the $U(1)$ gauge fields. It depends on the renormalization scale μ mildly, and its value at the electroweak scale will vary according to the free choice of the scale μ_0 where the mixing vanishes, $\eta(\mu_0) = 0$. For μ_0 chosen in the

range $[M_Z, M_{\text{GUT}}]$ one finds $\eta(M_Z) \in [0, 0.656]$ [37]. The largest value corresponds to a special case, where we assume that the kinetic mixing vanishes near the Planck scale.

The interaction vertices can be obtained using the implementation of the model [38] in SARAH [40–42]. For the Z' -neutrino interactions, we find

$$-ieC_{Z'\nu_i\nu_k}^L = -\frac{i}{2} \left[\sum_{j=1}^3 (\mathbf{U}_{i,j})(\mathbf{U}^\dagger)_{j,k} \left(\frac{e}{\sin\theta_W \cos\theta_Z} \sin\theta_Z + (\eta - 1)g_z \cos\theta_Z \right) \right] \quad (15)$$

$$-g_z \cos\theta_Z \sum_{j=1}^3 \mathbf{U}_{i,j+3}(\mathbf{U}^\dagger)_{j+3,k} \quad (16)$$

where θ_W is Weinberg's angle and \mathbf{U} is the neutrino mixing matrix. The model contains three extra heavy sterile right-handed neutrinos $N_{R,i}$ ($i = 1, 2, 3$), so this matrix is a 6×6 unitary matrix. The sterile neutrinos of the SWSM are much more massive than the active ones. We may safely assume that active-sterile neutrino mixing is negligible (that is, the off-diagonal 3×3 blocks vanish), and hence the active neutrino mixing matrix is unitary (the 3×3 upper left block of \mathbf{U} , ie. Pontecorvo-Maki-Nakagawa-Sakata matrix). Using these conditions, we can perform the matrix element sums and obtain the simplified expression:

$$-ieC_{Z'\nu\nu}^L \approx -\frac{i}{2} \left(\frac{e}{\sin\theta_W \cos\theta_Z} \sin\theta_Z + (\eta - 1)g_z \cos\theta_Z \right). \quad (17)$$

The other Z' -fermion couplings (multiplied by i for easier reading) are

$$eC_{Z'dd}^L \approx -\frac{1}{6} \tan\theta_W \left(e(3\cot^2\theta_W + 1) \sin\theta_Z + (\eta - 1)g_z \cot\theta_W \cos\theta_Z \right) \quad (18)$$

$$eC_{Z'dd}^R \approx +\frac{1}{6} \left(2e \tan\theta_W \sin\theta_Z + (2\eta - 5)g_z \cos\theta_Z \right) \quad (19)$$

$$eC_{Z'uu}^L \approx -\frac{1}{6} \tan\theta_W \left(e(1 - 3\cot^2\theta_W) \sin\theta_Z + (\eta - 1)g_z \cot\theta_W \cos\theta_Z \right) \quad (20)$$

$$eC_{Z'uu}^R \approx -\frac{1}{6} \left(4e \tan\theta_W \sin\theta_Z + (4\eta - 7)g_z \cos\theta_Z \right) \quad (21)$$

$$eC_{Z'ee}^L \approx -\frac{1}{2} \tan\theta_W \left(e(\cot^2\theta_W - 1) \sin\theta_Z - (\eta - 1)g_z \cot\theta_W \cos\theta_Z \right) \quad (22)$$

$$eC_{Z'ee}^R \approx +\frac{1}{2} \left(2e \tan\theta_W \sin\theta_Z + (2\eta - 3)g_z \cos\theta_Z \right) \quad (23)$$

Now we may write the Feynman amplitude for virtual Z' -mediated $\nu_\ell f \rightarrow \nu_\ell f$ -scattering. Then we obtain the NSI couplings derived from the SWSM as

$$\varepsilon^{f,X}(g_z, \eta, \tan\beta) = -\frac{v^2}{2(q^2 - M_{Z'}^2)} (eC_{Z'\nu\nu}^L)(eC_{Z'ff}^X), \quad (24)$$

which interpolates smoothly between the limits of heavy or light NSI couplings given by

$$\varepsilon^{f,X} \approx \frac{1}{2}(eC_{Z'\nu\nu}^L)(eC_{Z'ff}^X) \times \begin{cases} \frac{v^2}{M_{Z'}^2}, & \text{when } M_{Z'}^2 \gg q^2, \\ -\frac{v^2}{q^2}, & \text{when } M_{Z'}^2 \ll q^2. \end{cases} \quad (25)$$

These NSI couplings are flavour universal, hence we have suppressed the corresponding lower indices. Also, flavour is conserved.

The mass of the Z' in Eq. (24) is fixed according to Eq. (A.14) of Ref [37], reproduced in an equivalent form here:

$$M_{Z'}^2(g_z, \eta, \tan \beta) = \frac{g_z^2 v^2 \tan^2 \beta}{1 + \frac{1}{e}(2 - \eta)g_z \sin \theta_W \cos \theta_W}, \quad (26)$$

with $\tan \beta = w/v$ being the the ratio of the two VEVs. In addition, the mixing angle θ_Z also depends on the same parameters (see Eq. (A.13) of [37]),

$$\tan 2\theta_Z = \frac{(1 - \frac{\eta}{2}) \frac{g_z \cos \theta_W}{g_L}}{\frac{1}{4} - \left((1 - \frac{\eta}{2})^2 + \tan^2 \beta \right) \left(\frac{g_z \cos \theta_W}{g_L} \right)^2}. \quad (27)$$

B. Numerical estimates

Solving the Eq. (26) for g_z , we obtain for positive g_z that

$$\begin{aligned} g_z &= \frac{1}{4ev^2 \tan^2 \beta} \\ &\times \left(\sqrt{M_{Z'}^2 (16e^2 v^2 \tan^2 \beta + (\eta - 2)^2 M_{Z'}^2 \sin^2 (2\theta_W))} - (\eta - 2) M_{Z'}^2 \sin (2\theta_W) \right) \\ &\simeq \frac{3.94 \cdot 10^{-6}}{\tan \beta} \times \frac{M_{Z'}}{\text{MeV}} \end{aligned} \quad (28)$$

where we substituted $\eta = 0$ and took into account only the leading order contribution. We justify this by noting that in our investigation the dependence of η on other parameters is weak and its inclusion is manifested by multiplying the right hand side of Eq. (28) with a multiplicative factor of $\mathcal{O}(1)$. Similarly,

$$\theta_Z \approx (2 - \eta) \cos \theta_W \frac{g_z}{g_L} \simeq 1.354(2 - \eta)g_z = g_z \times \mathcal{O}(1). \quad (29)$$

Assuming $\theta_Z \ll 1$ (i.e. super-weak coupling), we can derive the following expressions for NSI couplings:

$$\varepsilon^u \simeq \frac{1}{2} \left(\frac{v}{M_{Z'}} \right)^2 \left(\frac{g_z^2}{12} (-5\eta^2 + 13\eta - 8) + 0.2355g_z\theta_Z(1.766 - \eta) + 0.0469\theta_Z^2 \right), \quad (30)$$

$$\varepsilon^d \simeq \frac{1}{2} \left(\frac{v}{M_{Z'}} \right)^2 \left(\frac{g_z^2}{12} (\eta^2 - 5\eta + 4) - 0.0626g_z\theta_Z(1.881 + \eta) - 0.0885\theta_Z^2 \right), \quad (31)$$

$$\varepsilon^e \simeq \frac{1}{2} \left(\frac{v}{M_{Z'}} \right)^2 \left(\frac{g_z^2}{4} (3\eta^2 - 7\eta + 4) + 0.5335g_z\theta_Z(1.338 - \eta) - 0.00536\theta_Z^2 \right). \quad (32)$$

Scanning over the possible η , we find

$$\theta_Z \in [1.820, 2.708]g_z \quad \text{and} \quad |\varepsilon^f| \in \text{in}_f \left(\frac{vg_z}{M_{Z'}} \right)^2, \quad (33)$$

with flavour dependent intervals

$$\text{in}_u = [0.248, 0.402], \quad \text{in}_d = [0.339, 0.651], \quad \text{in}_e = [0.4275, 1.486]. \quad (34)$$

Note that the NSI parameters are not independent of each other, which can be seen by taking the ratio of up- and down-type quark NSI in SWSM,

$$R = \frac{\varepsilon^u}{\varepsilon^d} = \frac{eC_{Z'uu}^L + eC_{Z'uu}^R}{eC_{Z'dd}^L + eC_{Z'dd}^R} = \frac{e(5 - 3\cot^2\theta_W)\sin\theta_Z + (5\eta - 8)g_z\cot\theta_W\cos\theta_Z}{e(3\cot^2\theta_W - 1)\sin\theta_Z - (\eta - 4)g_z\cot\theta_W\cos\theta_Z}, \quad (35)$$

from which we can express η as

$$\eta = \frac{\frac{e}{g_z} \tan\theta_W \tan\theta_Z (3(R+1)\cot^2\theta_W - R - 5) + 4R + 8}{R + 5}. \quad (36)$$

It turns out that the resulting valid benchmark points are confined to a very narrow region (see the next section).

Finally we remark that assuming a universal bound ε_{\max} for the NSI couplings, we may present a simple analytic bound in the $(M_{Z'}, g_z)$ plane, namely

$$g_z < \sqrt{\varepsilon_{\max}} \left(\frac{M_{Z'}}{v} \right) \times \mathcal{O}(1). \quad (37)$$

IV. RESULTS

Our results are two-fold. First we present constraints on the parameters of the SWSM and also on the NSI parameters originating from the SWSM. Next we discuss our predictions for those NSI couplings.

A. Free parameters and constraints

The NSI couplings depend on the gauge sector parameters g_z , η and on $\tan\beta$, which we choose as free parameters in the model. For the neutrino masses we consider, we may assume that the PMNS matrix is unitary, since nonunitary effects contributing to the NSI are negligible [39].

We scanned the $(\log_{10} \tan\beta, \log_{10} |g_z|, \eta)$ right rectangular prism by a uniformly distributed random sampling in $[-2, 2] \times [-10, 0] \times [0, 0.656]$ to determine the region consistent with current bound on isotropic NSI couplings, derived in Sec. 2.3. Larger values of $\tan\beta$ are possible in principle, but in such cases the new scalar sector decouples almost completely, hence remains inaccessible. Also values $\tan\beta \gtrsim 100$ are disfavored by the overproduction of dark matter if the SWSM is to explain the origin of dark matter energy density observed in the Universe [43]. We used the 2σ limits for the NSI couplings as given in Table III. We present the allowed values in histograms in Fig. 5 and in Table V. We see that the model prefers small values of $M_{Z'}$ and $\tan\beta$. The distribution of g_z (hence also θ_Z) is fairly flat within the allowed range $g_z \in 5 \cdot [10^{-6}, 10^{-4}]$ (approximately), with the full allowed range being somewhat larger. We note that the average value (or also the median) of the asymmetric ε^u and ε^d distributions are positive and negative, since they are skewed to the respective values.

B. Predictions

The NSI couplings ε^u and ε^d derived from the SWSM are anticorrelated, as can be seen on Fig. 6 obtained using those in Eq. (24) with $q^2 \simeq (51 \text{ MeV})^2$ as the characteristic energy transfer squared in the COHERENT experiment. The region between black lines is consistent with the 2σ bounds from COHERENT. The data points are coloured according to the mass of the Z' . Three distinct Z' mass regions emerge. In the lower right sector two clearly different Z' mass regions can be identified: light (turquoise) and heavy (red) areas. The region with red colour in the left plot is inconsistent SWSM freeze-out dark matter scenario, which requires that the mass of the Z' boson falls into the (10–135) MeV mass range [37]. Restricting our scan to this constrained region, shown on the right plot, reveals additional predictions: if $q \lesssim M_{Z'} \leq m_\pi$, then $\varepsilon_u < 0 < \varepsilon_d$ but if $10 \text{ MeV} \leq M_{Z'} \lesssim q$, then $\varepsilon_d < 0 < \varepsilon_u$.

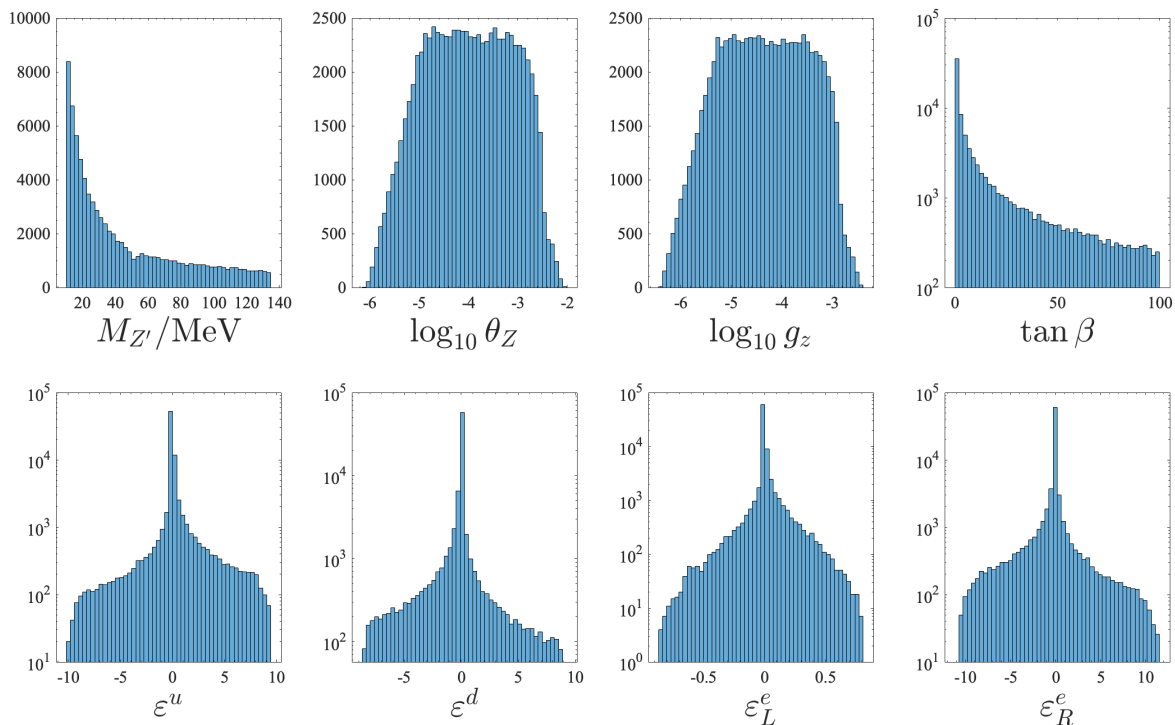


Figure 5. Histograms (containing 50 bins) of the scan (with total number of points $N = 10^6$) corresponding to $M_{Z'}$, $\log_{10} \theta_Z$, $\log_{10} g_z$, $\tan \beta$, ϵ^u , ϵ^d , ϵ_L^e and ϵ_R^e . Note that the first three of the histograms have linear, while the last five ones have logarithmic vertical axis.

In the left panel of Fig. 7 we can see that the parameter η is almost a linear function of the ratio (ϵ^u/ϵ^d) as one expects based on the discussion after Eq. (35). This information is visualized as a heat map in the right panel of Fig. 7, which shows that the COHERENT limits are compatible with $\epsilon^u > 0$ at the 2σ confidence level only for $\eta \lesssim 0.3$ at the electroweak scale. The region between dotted lines corresponds to 1σ bounds from COHERENT.

We present additional benchmark points (BPs) in Fig. 8 over the (g_z, X) planes ($X = \eta, \theta_Z$ and $M_{Z'}$) as heat maps depending on the mass of the Z' . All these plots are relevant in the context of explaining dark matter within the SWSM. The BPs do not exhibit any particular dependence on the parameter η representing the kinetic mixing. The second plot visualizes precisely the approximate relation in Eq. (29). We show the available parameter space in $(\tan \beta, g_z)$ plane separately in Fig. 9 where we present approximate analytic bounds superimposed (green dashes). In addition we added the NA64 constraint obtained by searching for dark photons, identified here with the Z' (red solid curve) [43]. For $\tan \beta$ we find the lower bounds corresponding to NA64

Parameter	Scan range	BP range (2σ)	BP range (1σ)
η	[0,0.656]	[0,0.656]	[0,0.656]
$\tan\beta$	[0.01,100]	[0.02,100]	[0.03,100]
$\log_{10} g_z$	[-10,1]	[-6.38, -2.31]	[-6.38, -2.41]
$M_{Z'}/\text{MeV}$	[10,135]	[10,135]	[10,135]
$\log_{10} \theta_Z$	–	[-6.09, -1.94]	[-6.09, -2.05]
ε^u	[-17.25, 17.16]	[-17.25, 17.16]	[-10.00, 9.42]
ε^d	[-15.31, 16.05]	[-15.31, 16.05]	[-8.606, 9.221]
ε_L^e	–	[-1.504, 1.462]	[-0.856, 0.808]
ε_R^e	–	[-19.87, 19.84]	[-10.91, 11.55]

Table V. Scan and benchmark point ranges corresponding 2 and 1σ allowed regions of COHERENT experiment.

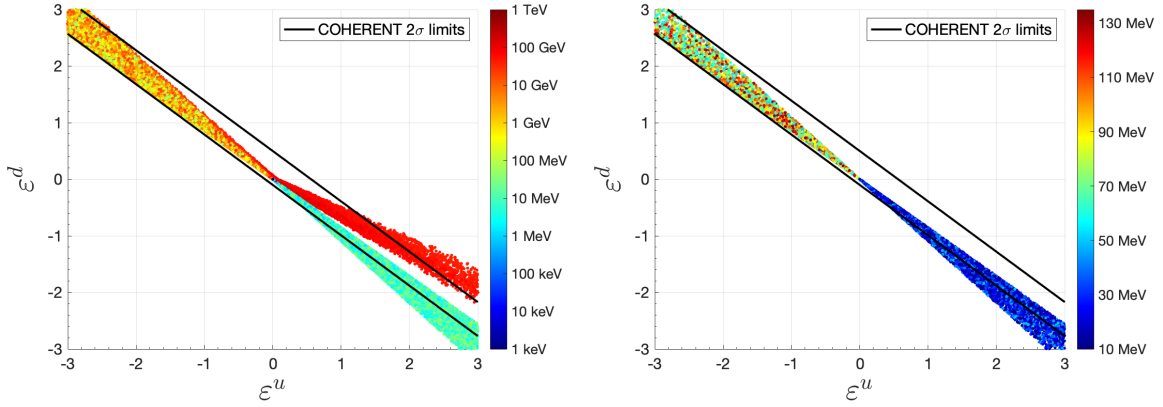


Figure 6. Left: Available parameter space in $(\varepsilon^u, \varepsilon^d)$ plane corresponding to the scan ranges in Table V except that for the mass of the Z' , for which $M_{Z'} \in [1, 10^9]$ keV. Right: benchmark points consistent with SWSM freeze-out dark matter scenario.

slightly depending on the value of the coupling g_z . The gauge coupling is constrained to 2σ confidence interval between $4.17 \cdot 10^{-6}$ and $4.90 \cdot 10^{-3}$, where the lower and upper bounds correspond to $M_{Z'} > 10$ MeV and $M_{Z'} < m_\pi$. We see that the mass of the Z' does not significantly affect this $\tan\beta$ bound, but the favoured values of θ_Z increase with $M_{Z'}$ (see Fig. 8).

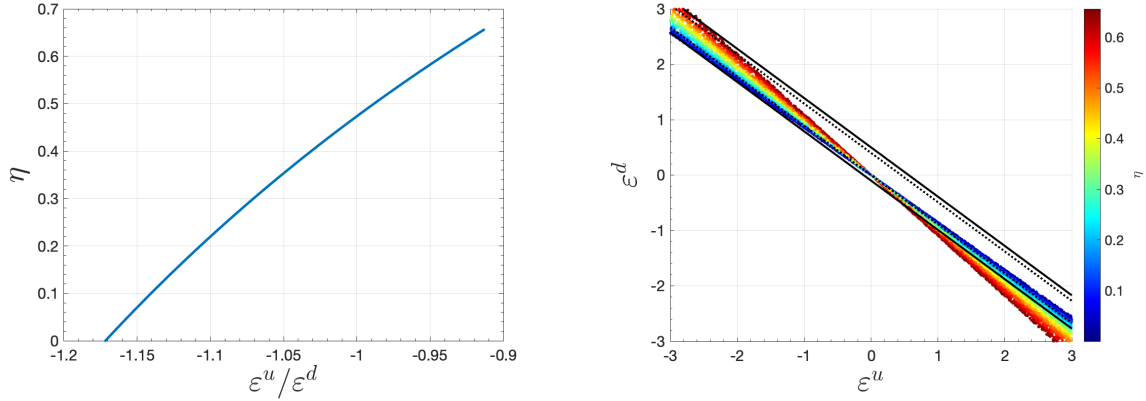


Figure 7. Left: The η parameter as a function of $\varepsilon^u/\varepsilon^d$. Right: As in Fig. 6 right panel, but the data points are coloured according to η , which corresponds to azimuthal angle in $(\varepsilon^u, \varepsilon^d)$ plane.

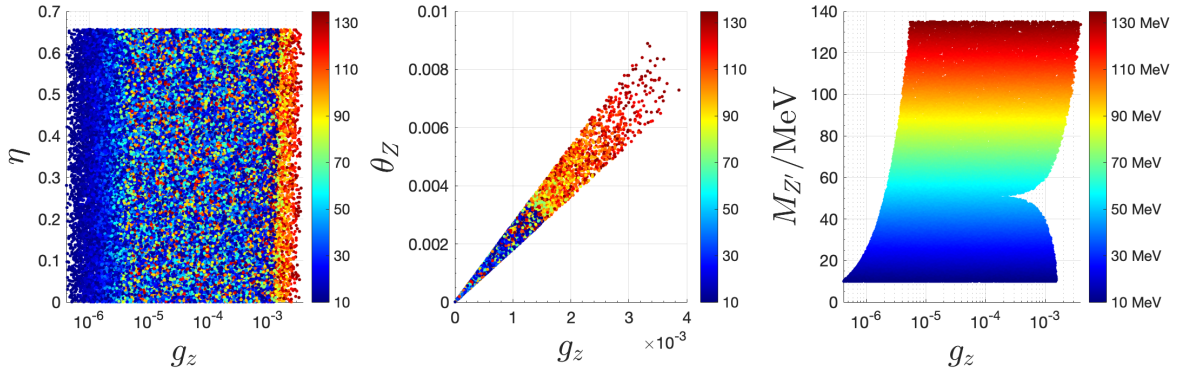


Figure 8. Benchmark points in (g_z, X) planes, with $X = \eta, \theta_Z$ and $M_{Z'}$. The colour corresponds to $M_{Z'}$ in MeV units.

While large NSI couplings are still allowed, according to Fig. 5 for the benchmark point distributions small couplings are favoured in $\varepsilon^u, \varepsilon^d, \varepsilon_L^e$ and ε_R^e . The corresponding BPs are shown in Fig. 10.

V. CONCLUSIONS AND FUTURE PROSPECTS

We have considered an exciting possibility for NSI, which escapes the high-energy experimental constraints and detection by neutrino oscillation experiments. Former experiments are unable to probe the interactions with a light mediator, while flavour-universal couplings between the mediator and a neutrino are manifested as an irrelevant

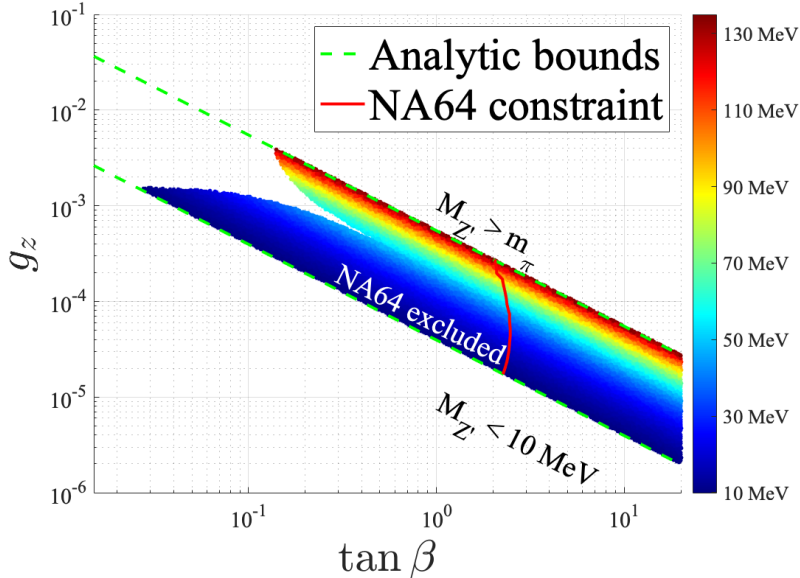


Figure 9. Available parameter space in $(\tan \beta, g_z)$ plane, where colour corresponds to $M_{Z'}$. Lower and upper analytic bounds for $M_{Z'}$ obtained from Eq. (28) using the allowed region for $M_{Z'}$ assuming the freeze-out dark matter scenario of SWSM [37]. The solid red line represents the NA64 constraint on direct dark photon search.

phase factor in neutrino oscillation Hamiltonian. In the presence of sterile neutrinos the factor does not disappear, but is suppressed [44].

The only viable avenue to probe flavour-universal light NSI couplings is then to consider $CE\nu$ NS. We derived the bounds for flavour-universal NSI both in light and heavy mediator case, and found that large NSI couplings ($\varepsilon \simeq 10$) are allowed for the light NSI scenario, while $\varepsilon \lesssim 10^{-2}$ for the heavy case.

We then considered a specific model, the super-weak extension of the standard model. We obtained the NSI couplings in the SWSM, which allowed us to investigate the parameter space of the SWSM as allowed by the existing constraints of $CE\nu$ NS on the NSI parameters. We found that in this range the model prefers small values for the mass of the new gauge boson and also for the ratio w/v of the VEVs. The kinetic mixing parameter is weakly constrained, but we found that its possible values are compatible with $\varepsilon^u/\varepsilon^d \in [-1.17, -0.92]$. This ratio of NSI strengths is a testable prediction of the SWSM. If we added the constraint set by the NA64 experiment on the mass of dark photon, we could constrain further the viable parameter space to $\tan \beta \gtrsim 2$ and $g_z \sim 10^{-6} - 10^{-3}$.

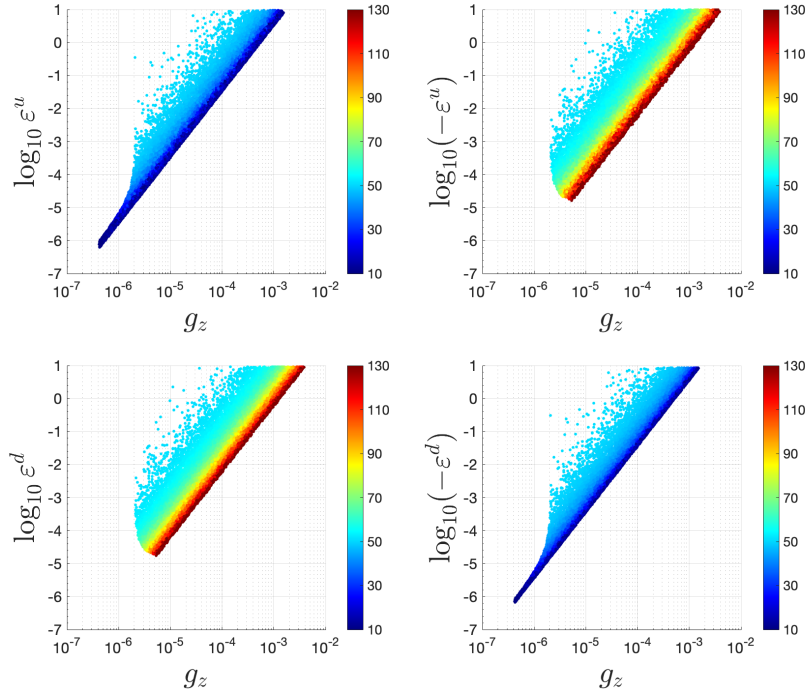


Figure 10. Benchmark points in $(g_z, \log_{10}(\pm\varepsilon^u))$ and $(g_z, \log_{10}(\pm\varepsilon^d))$ planes. Note that different signs of the NSI parameters correspond to two regions of parameter space: $M_{Z'} < 51$ MeV and $M_{Z'} > 51$ MeV. We separated the cases corresponding to positive and negative values of ε^u and ε^d . The colour corresponds to $M_{Z'}$.

Our study demonstrated that even low-energy experiments have significant potential on constraining new physics discovery. Both higher-intensity and higher-energy experiments are needed for the progressive discovery of light and heavy NSI interactions. While the limits from CE ν NS are quite loose at present, their expected improvement at the ESS [20] will constrain the parameter space of the SWSM severely.

-
- [1] Y. Fukuda *et al.* (Super-Kamiokande), *Phys. Rev. Lett.* **81**, 1562 (1998), [arXiv:hep-ex/9807003 \[hep-ex\]](#).
 - [2] Q. R. Ahmad *et al.* (SNO Collaboration), *Phys. Rev. Lett.* **87**, 071301 (2001).
 - [3] H. Fritzsch, M. Gell-Mann, and P. Minkowski, *Physics Letters B* **59**, 256 (1975).
 - [4] P. Minkowski, *Phys. Lett.* **67B**, 421 (1977).
 - [5] M. Gell-Mann, P. Ramond, and R. Slansky, *Supergravity Workshop Stony Brook, New York, September 27-28, 1979*, *Conf. Proc.* **C790927**, 315 (1979), [arXiv:1306.4669 \[hep-](#)

- th].
- [6] T. Yanagida, *Proceedings: Workshop on the Unified Theories and the Baryon Number in the Universe: Tsukuba, Japan, February 13-14, 1979*, Conf. Proc. **C7902131**, 95 (1979).
 - [7] R. N. Mohapatra and G. Senjanović, *Phys. Rev. Lett.* **44**, 912 (1980).
 - [8] R. N. Mohapatra and G. Senjanovic, *Phys. Rev.* **D23**, 165 (1981).
 - [9] J. Schechter and J. W. F. Valle, *Phys. Rev.* **D22**, 2227 (1980).
 - [10] M. Magg and C. Wetterich, *Phys. Lett.* **94B**, 61 (1980).
 - [11] S. L. Glashow, *Cargese Summer Institute: Quarks and Leptons Cargese, France, July 9-29, 1979*, *NATO Sci. Ser. B* **61**, 687 (1980).
 - [12] G. Lazarides and Q. Shafi, *Phys. Lett.* **99B**, 113 (1981).
 - [13] G. B. Gelmini and M. Roncadelli, *Phys. Lett.* **99B**, 411 (1981).
 - [14] R. Foot, H. Lew, X. G. He, and G. C. Joshi, *Zeitschrift für Physik C Particles and Fields* **44**, 441 (1989).
 - [15] R. N. Mohapatra and A. Y. Smirnov, *Ann. Rev. Nucl. Part. Sci.* **56**, 569 (2006), [arXiv:hep-ph/0603118](#).
 - [16] S. F. King, A. Merle, S. Morisi, Y. Shimizu, and M. Tanimoto, *New J. Phys.* **16**, 045018 (2014), [arXiv:1402.4271 \[hep-ph\]](#).
 - [17] S. F. King, *Rept. Prog. Phys.* **67**, 107 (2004), [arXiv:hep-ph/0310204](#).
 - [18] S. Weinberg, *Phys. Rev. Lett.* **43**, 1566 (1979).
 - [19] Y. Grossman, *Phys. Lett.* **B359**, 141 (1995), [arXiv:hep-ph/9507344 \[hep-ph\]](#).
 - [20] D. Baxter *et al.*, *JHEP* **02**, 123, [arXiv:1911.00762 \[physics.ins-det\]](#).
 - [21] D. Z. Freedman, *Phys. Rev. D* **9**, 1389 (1974).
 - [22] D. Akimov *et al.* (COHERENT), *Science* **357**, 1123 (2017), [arXiv:1708.01294 \[nucl-ex\]](#).
 - [23] D. Akimov *et al.* (COHERENT), *Phys. Rev. Lett.* **126**, 012002 (2021), [arXiv:2003.10630 \[nucl-ex\]](#).
 - [24] J. Dorenbosch *et al.* (CHARM), *Phys. Lett. B* **180**, 303 (1986).
 - [25] G. P. Zeller *et al.* (NuTeV), *Phys. Rev. Lett.* **88**, 091802 (2002), [Erratum: *Phys.Rev.Lett.* **90**, 239902 (2003)], [arXiv:hep-ex/0110059](#).
 - [26] L. B. Auerbach *et al.* (LSND), *Phys. Rev. D* **63**, 112001 (2001), [arXiv:hep-ex/0101039](#).
 - [27] Z. Trócsányi, *Symmetry* **12**, 107 (2020), [arXiv:1812.11189 \[hep-ph\]](#).
 - [28] P. B. Denton, Y. Farzan, and I. M. Shoemaker, *JHEP* **07**, 037, [arXiv:1804.03660 \[hep-ph\]](#).

- [29] C. Giunti, *Phys. Rev. D* **101**, 035039 (2020), [arXiv:1909.00466 \[hep-ph\]](#).
- [30] Z. Péli and Z. Trócsányi, *Phys. Rev. D* **106**, 055045 (2022), [arXiv:2204.07100 \[hep-ph\]](#).
- [31] P. Coloma, P. B. Denton, M. C. Gonzalez-Garcia, M. Maltoni, and T. Schwetz, *JHEP* **04**, 116, [arXiv:1701.04828 \[hep-ph\]](#).
- [32] J. A. Koziol and M. D. Perlman, *Journal of the American Statistical Association* **73**, 753 (1978).
- [33] J. Barranco, O. G. Miranda, C. A. Moura, and J. W. F. Valle, *Phys. Rev. D* **77**, 093014 (2008), [arXiv:0711.0698 \[hep-ph\]](#).
- [34] S. K. Agarwalla *et al.* (Borexino), *JHEP* **02**, 038, [arXiv:1905.03512 \[hep-ph\]](#).
- [35] C. Biggio, M. Blennow, and E. Fernandez-Martinez, *JHEP* **08**, 090, [arXiv:0907.0097 \[hep-ph\]](#).
- [36] P. Coloma, M. C. Gonzalez-Garcia, M. Maltoni, and T. Schwetz, *Phys. Rev. D* **96**, 115007 (2017), [arXiv:1708.02899 \[hep-ph\]](#).
- [37] S. Iwamoto, K. Seller, and Z. Trócsányi, *JCAP* **01** (01), 035, [arXiv:2104.11248 \[hep-ph\]](#).
- [38] S. Iwamoto, T. J. Kärkkäinen, Z. Péli, and Z. Trócsányi, *Phys. Rev. D* **104**, 055042 (2021), [arXiv:2104.14571 \[hep-ph\]](#).
- [39] T. J. Kärkkäinen and Z. Trócsányi, *J. Phys. G* **49**, 045004 (2022), [arXiv:2105.13360 \[hep-ph\]](#).
- [40] F. Staub, *Comput. Phys. Commun.* **181**, 1077 (2010), [arXiv:0909.2863 \[hep-ph\]](#).
- [41] F. Staub, *Comput. Phys. Commun.* **182**, 808 (2011), [arXiv:1002.0840 \[hep-ph\]](#).
- [42] F. Staub, *Comput. Phys. Commun.* **185**, 1773 (2014), [arXiv:1309.7223 \[hep-ph\]](#).
- [43] K. Seller, *PoS ICHEP2022*, 290 (2022), [arXiv:2210.16090 \[hep-ph\]](#).
- [44] T. J. Kärkkäinen and Z. Trócsányi, *Acta Phys. Polon. Supp.* **15**, 1 (2022), [arXiv:2111.07789 \[hep-ph\]](#).